

1 **Regional Frequency Analysis at Ungauged Sites with Multivariate**
2 **Adaptive Regression Splines.**

3
4
5
6
7
8

A. Msilini^{*,1}, P. Masselot¹, T.B.M.J. Ouarda¹

9 ¹ Canada Research Chair in Statistical Hydro-Climatology, INRS-ETE, 490 de la
10 Couronne, Québec, QC, G1K 9A9, Canada

11
12
13

14 * Corresponding author: Amina Msilini (Amina.Msilini@ete.inrs.ca).

15
16
17
18
19
20
21
22
23
24
25

26 March, 2020

27 **Abstract**

28 Hydrological systems are naturally complex and nonlinear. A large number of
29 variables, many of which not yet well considered in regional frequency analysis (RFA),
30 have a significant impact on hydrological dynamics and consequently on flood quantile
31 estimates. Despite the increasing number of statistical tools used to estimate flood
32 quantiles at ungauged sites, little attention has been dedicated to the development of new
33 regional estimation (RE) models accounting for both nonlinear links and interactions
34 between hydrological and physio-meteorological variables. The aim of this paper is to
35 simultaneously take into account non-linearity and interactions between variables by
36 introducing the multivariate adaptive regression splines (MARS) approach in RFA. The
37 predictive performances of MARS are compared with those obtained by one of the most
38 robust RE models: the generalized additive model (GAM). Both approaches are applied
39 to two datasets covering 151 hydrometric stations in the province of Quebec (Canada): a
40 standard dataset (STA) containing commonly used variables and an extended dataset
41 (EXTD) combining STA with additional variables dealing with drainage network
42 characteristics. Results indicate that RE models using MARS with the EXTD outperform
43 slightly RE models using GAM. Thus MARS seems to allow for a better representation
44 of the hydrological process and an increased predictive power in RFA.

45

46

47

48 **1. Introduction and literature review**

49 The main objective of regional frequency analysis (RFA) is the estimation of the
50 return period of extreme hydrological events at target sites where little or no hydrological
51 data is available. Examples of these events include floods and low-flow quantiles which
52 are crucial for infrastructure design and management. In general, RFA comprises two
53 main steps: i) the delineation of homogenous region (DHR) to determine gauged sites
54 similar to the target one and ii) regional estimation (RE) to transfer the information from
55 sites determined in the DHR step to the target one (e.g. Chebana and Ouarda, 2008).
56 Various methods have been suggested for each of these two steps (e.g. Ouarda, 2016).

57 Among the most common DHR methods, we can mention the region of influence
58 (ROI) (Burn, 1990a) and the canonical correlation analysis (CCA) (Ouarda et al., 2001).
59 Recently, several advanced non-linear neighborhood approaches were suggested (e.g.
60 Ouali et al., 2016; Wazneh et al., 2016). Among the commonly used RE approaches, we
61 can distinguish the regression-based models and the index-flood models. Among the
62 former, the log-linear regression models are the most commonly used ones in practice,
63 because of their simplicity and good predictive performances. We focus here on
64 regression-based models in the RE step.

65 Hydrological processes depend from a large number of variables, such as the
66 topographic variability of the basins, their soil structure and texture, their geological
67 formations and the climatology. This leads to a natural complexity, which has been
68 widely recognized and documented in the hydrological literature (e.g. Ibbitt and Woods,
69 2004; Sivakumar, 2007; W. Wang et al., 2008; Xu et al., 2010). In statistical terms, this

70 complexity manifests itself through three aspects: i) the high number of explanatory
71 variables necessary to paint a realistic picture of the processes, ii) the nonlinear impact of
72 these explanatory variables and iii) the important interaction between the different
73 explanatory variables. It is thus important that the RE step in RFA accounts for these
74 three aspects in order to yield accurate estimations of the target site's quantiles of
75 interest.

76 In RFA studies, the RE step usually requires a large number of explanatory
77 variables to result in satisfactory predictive performances. This number usually exceeds
78 five, as in Ouarda et al. (2018), but should increase in the future with the discovery of
79 new potential variables. For instance, evidence is growing that drainage network
80 characteristics have a strong impact on hydrological dynamics, and are consequently
81 linked to flood quantiles (Jung et al., 2017). Thus, integrating additional characteristics
82 related to the drainage network may lead to more accurate estimates of the regional
83 quantiles. Hence, there is a need to propose efficient approaches that are able to manage
84 such high-dimensional databases.

85 Another consequence of the natural complexity of hydrological processes is the
86 nonlinearity between explanatory variables and the at-site quantiles. To handle this
87 problem and better reproduce the dynamics of hydrological processes, various non-linear
88 approaches have been proposed (e.g. Shu and Burn, 2004). The classical log-linear
89 method used in the RE step assumes that the relation between the logarithm of the
90 response variable (hydrological) and explanatory variables (physio-meteorological) is
91 linear, which is too simplistic for such complex non-linear processes. Therefore, several
92 RE approaches, such as random forest (RF), artificial neural network (ANN), and

93 generalized additive models (GAM) have been proposed in the literature to account for
94 the possible nonlinear links between variables (e.g. Aziz et al., 2014; Khalil et al., 2011;
95 Ouali et al., 2017; Ouarda et al., 2018; Saadi et al., 2019).

96 Random forest (Breiman, 2001), is a powerful nonlinear and non-parametric
97 method commonly used to handle regression and classification problems based on
98 decision trees. Due to its good performance, it has been applied in several fields, such as
99 hydrology (e.g. Diez-Sierra and del Jesus, 2019; Muñoz et al., 2018; Z. Wang et al.,
100 2015), ecology (e.g. Cutler et al., 2007; Prasad et al., 2006) environmental modeling (e.g.
101 Masselink et al., 2017; Pourghasemi and Kerle, 2016) and RFA (e.g. Booker and Woods,
102 2014; Brunner et al., 2018). Despite its predictive power, RF suffers from major
103 limitations such as the difficulty of interpretation and the large memory requirements for
104 storing the model when used with a large dataset (Geurts et al., 2009).

105 The ANN is a nonparametric mathematical model, whose design is inspired by the
106 biological functioning of brain neurons (Bishop, 1995). It was considered in several RFA
107 studies for the estimation of flood and low-flow quantiles at ungauged sites (e.g. Aziz et
108 al., 2014; Ouarda and Shu, 2009). However, ANNs present a major common problem
109 which is the tendency to overfit (e.g. Gal and Ghahramani, 2016; Lawrence and Giles,
110 2000). In addition, their calibration is relatively complex, especially for debutant users,
111 which requires some subjective choices since no explicit regression equations can be
112 given (Ouali et al., 2017).

113 GAMs do not suffer the same drawbacks as ANNs. GAMs are flexible nonlinear
114 regression models (Hastie and Tibshirani, 1987), that have been introduced in the RFA

115 context by Chebana et al. (2014). The authors found that the GAM-based methods
116 present the best performances when compared to the classical log-linear model and other
117 common methods. GAMs are increasingly being adopted in several fields such as hydro-
118 climatology and environmental modeling (e.g. Rahman et al., 2018; Wen et al., 2011),
119 public health (e.g. Bayentin et al., 2010; Leitte et al., 2009), and renewable energy (e.g
120 Ouarda et al., 2016). However, it still presents a number of disadvantages. Indeed, the
121 method can be computationally intensive, especially when a large number of variables is
122 involved. It can, then, be difficult to fit GAM to high-dimensional databases because of
123 memory limitations imposed by the numerical complexities of this model (Leathwick et
124 al., 2006). More importantly, GAMs do not cope well with the interaction between
125 variables (e.g. Ramsay et al., 2003), which is difficult to integrate in the model.

126 The interaction between physiographical variables within the watershed has long
127 been recognized (e.g. Niehoff et al., 2002). Thus, the inclusion of the terms of
128 interactions between the explanatory variables used to model the hydrological dynamics
129 seems to be essential for better estimates of flood quantiles. However, this aspect is
130 difficult to take into account in the RE models due to the high complexity that it may add
131 to the models (see above for the specific example of GAMs). This affects the quality of
132 the estimates and makes it less accurate. Hence, the motivation behind the present paper
133 is to propose and explore alternative techniques able to realistically reproduce the
134 hydrological process while avoiding the problems mentioned above.

135 The method considered here is multivariate adaptive regression splines (MARS), a
136 procedure designed to build complex nonlinear regression models in a high dimensional
137 setting. It is attractive in the RFA context since it actually addresses the three issues

138 developed above which are: high number of variables, nonlinearity, and interactions.
139 Indeed, MARS is efficient in a high dimensional setting and naturally selects the relevant
140 predictors in this context. In addition, it does not require assumptions about the form of
141 the relationships between the response and the explanatory variables (Friedman, 1991).
142 MARS also allows the modelling of complex structures between variables, which are
143 often hidden in high-dimensional data, without imposing strong model assumptions.
144 Hence, it can easily include interactions between variables, allowing any degree of
145 interaction to be considered (Lee et al., 2006).

146 All of these desirable properties lead to a very flexible approach able to adapt well
147 to the hydrological phenomenon. Due to its simplicity and capacity to capture complex
148 nonlinear relationships, it has been successfully applied in several fields such as ecology
149 and environment (e.g. Balshi et al., 2009; Bond and Kennard, 2017; Leathwick et al.,
150 2006; Leathwick et al., 2005), finance (e.g. Lee and Chen, 2005; Lee et al., 2006),
151 geology (e.g. Zhang and Goh, 2016; Zhang et al., 2015), energy (e.g. Li et al., 2016; Roy
152 et al., 2018) and hydrology (e.g. Bond and Kennard, 2017; Deo et al., 2017;
153 Emamgolizadeh et al., 2015; Kisi, 2015; Kisi and Parmar, 2016). Despite the extensive
154 use of the MARS model in various frameworks and contexts, its potential has never been
155 exploited and investigated in the context of RFA of extreme hydrological events.

156 The main objective of the present study is to introduce the MARS approach in the
157 RFA context to estimate flood quantiles and evaluate its predictive potential when it is
158 applied to an extensive database. It is hereby applied in combination with the DHR with
159 the CCA and the ROI approaches. MARS is also applied without DHR to test its
160 performance when applied to all stations without consideration of hydrological

161 neighborhoods. A jackknife procedure is used to evaluate the model performances, with
162 GAMs used as a benchmark.

163 This paper is structured as follows. Section 2 presents the theoretical background of
164 MARS and the other RFA approaches adopted. The considered methodology is outlined
165 in section 3. Section 4 describes the case study and the considered datasets. The obtained
166 results are presented and discussed in section 5. The conclusions of the study are
167 summarized in the last section.

168 **2. Theoretical background**

169 In this section, the adopted statistical tools are briefly presented and discussed.

170 **2.1 Neighborhood identification approaches**

171 Here we present the two most commonly considered neighborhood identification
172 approaches as a necessary step before the RE one.

173 **2.1.1 Canonical correlation analysis (CCA) approach**

174 CCA (Hotelling, 1935) is a multivariate analysis technique used to identify the
175 possible correlations between two groups of variables. It consists of a linear
176 transformation of two groups of random variables into pairs of canonical variables, which
177 are established in such a way that the correlations between each pair are maximized.

178 Let $X = (X_1, X_2, \dots, X_r)$ and $Y = (Y_1, Y_2, \dots, Y_s)$ be sets of random variables including,
179 respectively, the r physio-meteorological variables and the s hydrological variables of

180 n gauged sites. The objective of CCA is to construct linear combinations V_i and
 181 W_i (called canonical variables) of the variables X and Y , i.e.:

$$V_i = A_{i1}X_1 + A_{i2}X_2 + \dots + A_{ir}X_r \quad (1)$$

$$W_i = B_{i1}Y_1 + B_{i2}Y_2 + \dots + B_{is}Y_s \quad (2)$$

182 where $i = 1, \dots, p$, with $p = \min(r, s)$. The first weights vectors A_1 and B_1 maximize the
 183 correlation coefficients between resulting canonical variables, i.e. $\lambda_1 = \text{corr}(V_1, W_1)$,
 184 under constraints of unit variance. Once the first pair of canonical variables is identified,
 185 other pairs $(V_i, W_i, i > 1)$ can be obtained under the constraint $\text{corr}(V_i, W_j) = 0$ (where $i \neq$
 186 j).

187 For neighbourhood delineation in RFA, the considered X_r are physio-
 188 meteorological variables while the Y_s are the flood quantiles of interest. CCA is then used
 189 to construct canonical variables W_i that correlate well with physio-meteorological
 190 variables. The neighbourhood is the set of sites such that the canonical hydrological score
 191 $w_k, k = 1, \dots, K$, is close to the canonical physio-meteorological score of the target
 192 ungauged site v_0 . The distance is measured by a Mahalanobis distance between the
 193 hydrological mean position of the target site Λv_0 and the positions of other sites w_k ,
 194 where $\Lambda = \text{diag}(\lambda_1, \dots, \lambda_p)$ and v_0 is the physio-meteorological canonical score of the
 195 target site. Provided the X variables are approximately normal, the Mahalanobis distance
 196 converges to a χ^2 distribution with p degrees of freedom. The size of the neighborhood is
 197 controlled by the parameter α that represent the $(1 - \alpha)$ χ_p^2 quantile above which sites
 198 are excluded from the neighborhood. As extreme cases, all stations are considered if $\alpha =$

199 0, and no station is included in the neighborhood when $\alpha = 1$. For more details the reader
200 is referred to Ouarda et al. (2001).

201 **2.1.2 Region of influence (ROI) approach**

202 The ROI approach was introduced by Burn (1990b), to identify the neighborhood
203 of a given target-site based on the similitude between watersheds characteristics. The
204 similitude is measured using an Euclidean distance in the multidimensional physio-
205 meteorological space (e.g. Burn, 1990b; Tasker et al., 1996) i.e.:

$$ROI_i = \left\{ \text{sites } j \in (1, \dots, n); D_{ij} = \left[\sum_{k=1}^r W_k (X_{k,i} - X_{k,j})^2 \right]^{\frac{1}{2}} \leq \theta \right\} \quad (3)$$

206 where D_{ij} is the weighted Euclidean distance between the target site i and the gauged
207 one, $j = 1, \dots, n$, $X_{k,j}$ ($k = 1, \dots, r$) is the standardized value of the k^{th} variable at site j , W_k
208 is the weight associated with the k^{th} variable, and θ represents the threshold value. The
209 threshold value is defined for each site in such a way that it permits a compromise
210 between the amount of information to be used and the degree of hydrological
211 homogeneity of the neighborhood (Ouarda et al., 1999). For more details, the reader is
212 referred to (e.g. Burn, 1990b; GREHYS, 1996).

213 **2.2 Regional estimation approaches**

214 Once a neighborhood is identified, the methods described below are used to transfer
215 information from the neighborhood stations to the target site.

216 **2.2.1 Generalized Additive Model (GAM)**

217 GAM (Hastie and Tibshirani, 1987) is a flexible class of nonlinear models that is able to
218 efficiently model a wide variety of nonlinear relationships. In addition, it allows for non-
219 gaussian response variables (Wood, 2006) making it relevant for streamflow data. Thus,
220 GAM allows a more realistic description of the hydrological phenomenon because of the
221 flexible non-parametric fitting of the smooth functions.
222 Formally, a GAM is defined as (Wood, 2006):

$$g(Y) = \alpha + \sum_{j=1}^m f_j(X_j) + \varepsilon \quad (4)$$

223 where g is a monotonic link function and f_j are smooth functions giving the relationship
224 between the explanatory variables X_j and the response Y . α is the intercept and ε is the
225 error term. The structure of eq. 4 allows for a distinct interpretation of each explanatory
226 variable.

227 To estimate the model, the smooth functions f_j are expressed as a set of q spline basis
228 functions, a common choice for smoothing (Wahba, 1990). They are expressed as:

$$f_j(X) = \sum_{i=1}^q \beta_{ji} b_{ji}(X) \quad (5)$$

229 where β_{ji} are unknown parameters to be estimated and b_{ji} are the spline basis functions.
230 The expansion in (5) allows linearizing the model that can then be estimated through
231 backfitting (Hastie and Tibshirani, 1987) or simple penalized least-squares (Wood, 2004).

232 For more details, the reader is referred to (e.g. Wood, 2006; Wood, 2017).

233 2.2.2 Multivariate adaptive regression splines (MARS)

234 MARS was introduced by Friedman (1991) as a flexible non-parametric regression
235 approach able to deal with high-dimensional data. The MARS model $f(X)$ can be seen as
236 a flexible extension of GAM, in that it is expressed as a linear combination of basis
237 functions and their interactions as:

$$f(X) = \beta_0 + \sum_{n=1}^r \beta_n B_n(X) \quad (6)$$

238 where β_0 is the intercept, β_n are regression coefficients of the basis functions ($B_n(X)$). In
239 the MARS model, the $B_n(X)$ terms can take one of the following forms: i) a constant
240 (just one term) which represent the intercept, ii) a linear spline functions on a single
241 variable X_j called hinge function, i.e. of the form $h_m(X_j) = (t_m - X_j)_+$ or $h_m(X_j) =$
242 $(X_j - t_m)_+$ where t is a knot and iii) a products of two or more hinge functions, e.g.
243 $B_n(X) = h_m(X_j)h_{m'}(X_k)$ where $j \neq k$. The latter represent interaction between two or
244 more variables. The $B_n(X)$ are defined in pairs and separated by a knot which represents
245 an inflection point along the range of a given explanatory variable (see Figure 1).
246 Allowing the product of several linear spline terms $h_m(X_j) = (t_m - X_j)_+$ as basis
247 functions further allows the integration of interaction in the model, an aspect GAMs are
248 not well designed for.

249 In mathematical terms, the hinge functions $h_m(X_j)$ are defined as (Rounaghi et al.,
250 2015):

$$(t - X_j)_+ = \begin{cases} t - X_j, & \text{if } t > X_j \\ 0, & \text{otherwise} \end{cases} \quad (7)$$

251

$$(X_j - t)_+ = \begin{cases} X_j - t, & \text{if } X_j > t \\ 0, & \text{otherwise} \end{cases} \quad (8)$$

252 where t is the knot position.

253 The main difference of MARS with GAM is in the estimation algorithm. Where the
254 spline bases are defined *a priori* in GAM, they are iteratively constructed in MARS,
255 adapting hence to the data. Indeed, building the model in (6) is carried out through two
256 phases: i) a forward addition of linear spline terms (i.e. of the form (7) and (8)) to build a
257 large model and ii) a backward deletion to delete irrelevant terms. The forward phase
258 begins with an empty model containing only the intercept β_0 . B_n s are then iteratively
259 added to the model, each time choosing the variable and knot yielding the largest
260 decrease in the residual error of the model. This process of adding B_n s continues until the
261 model reaches some predetermined maximum number, leading to a large model which
262 may over-fit the data. A backward deletion phase is then performed to improve the model
263 performance by removing the less significant B_n s until obtaining the best sub-models.
264 Comparison of sub-models is made based on the Generalized Cross Validation (GCV).
265 Figure 2 illustrates the details of the MARS model algorithm.

266 Another interesting feature of MARS is the assessment of the variable importance
267 for the prediction of the response. Variable importance can be measured in two different

268 ways: i) the number of sub-models that include the variable, or ii) the increase in GCV
269 caused by deleting the considered variables from the final MARS model (e.g. Roy et al.,
270 2018).

271 **3. Methodology**

272 **3.1 Regional models**

273 In this study, the methods presented in section 2 for neighborhood delineation
274 (CCA and ROI) are used in combination with the regional estimation models GAM and
275 MARS for transfer of hydrological information. As mentioned in section 1, other
276 evaluated models are obtained by applying the GAM and MARS using all stations, i.e.
277 without defining any neighborhoods. Table 1 summarizes all six resulting combinations.

278 The two most commonly used neighborhood approaches, the CCA and the ROI
279 (Ouarda, 2016) are applied to the DHR using two sets of variables. For these methods,
280 the relevant variables are selected based on their correlation degree with the hydrological
281 variables.

282 Considering the classical procedures used to define the threshold in ROI and CCA,
283 the density of stations in the neighborhoods can vary considerably from one region to
284 another. Indeed, for a given fixed threshold, stations located near the center of the cloud
285 points defined by the canonical space for CCA or the Euclidean space for ROI will have
286 more stations within their neighbourhoods and vice versa (Leclerc and Ouarda, 2007).
287 Since, the sample may affect the accuracy of the estimates obtained by regression
288 models, it was decided that for each target station, the size of the region is increased until

289 a selected optimal size is reached. The optimal number of stations to be considered in the
290 DHR step is chosen based on the optimization procedure of Ouarda et al. (2001). The
291 optimal number of sites in the neighborhood is the one that minimizes a given
292 performance criterion of the log-linear model applied in each neighborhood.

293 MARS is fitted using the R package *earth* (Milborrow, 2018). The application of
294 MARS needs the tuning of three main parameters (see Figure 2): the maximum number
295 of terms in the model in the forward phase (N_k), the degree of interaction (degree), and
296 the maximum number of terms in the Backward phase (N_{prune}). A range of values of
297 these parameters was tested and evaluated in order to optimize them based on the
298 GCV, the residual sum of squares (RSS) and the coefficient of determination (R^2) criteria
299 of the fitted models.

300 GAM is also implemented on R, through the package *mgcv* (Wood, 2006). The thin
301 plate regression spline is used in this study as basis b_{ji} in the smoothing function f_j in
302 (5). The latter is selected due to its advantages, i.e. low calculation time, flexibility and
303 fewer number of parameters compared to other smoothing functions (Wood, 2003). The
304 used link function g in (4) is the identity function because of the approximately normal
305 log-transformed quantiles such as considered in Ouali et al. (2017).

306 Different physio-meteorological variables are considered in each regional model. A
307 backward stepwise approach is applied in this study to select the relevant explanatory
308 variables to be used in each RE models (GAM and MARS). This method is presented in
309 the next section.

310 **3.2 Variable selection**

311 The backward stepwise selection procedure is applied in this work to select the
312 optimal explanatory variables as in Ouarda et al. (2018) and Chebana et al., (2014). It
313 consists in a progressive deleting of the least effective variables from an initial full model
314 containing all available variables. At each step, the removed variable is the one having
315 either the highest p value for the null hypothesis that the smooth term for GAM is zero or
316 those whose consideration yields the most significant increase in the GCV score of the
317 model for MARS.

318 Note that the MARS algorithm naturally includes a variable selection feature since
319 it builds a sparse model and a variable for which no term is added is by default discarded.
320 This is not the case for GAM within which an automatic backward stepwise procedure
321 was specially developed for this study.

322 **3.3 Validation**

323 For each RFA combination in Table 1, performances are evaluated using a leave-
324 one-out cross validation, commonly called jackknife procedure in the field of hydrology.
325 It consists in deleting temporarily each site to consider it the target one and perform RE.
326 This process is repeated for each gauged sites. Then, the regional estimate is compared to
327 its observed values. Note that, in statistics, the validation with the jackknife technique is
328 carried out on the retained data not on the data removed as in the leave-one-out cross
329 validation (Quenouille, 1949). However, we will retain the jackknife term for ease of
330 presentation.

331 Based on the jackknife procedure, several standard performance criteria are used to
332 evaluate the prediction power of each regional model (e.g. Ouali et al., 2016). First, the
333 Nash criterion (NASH) gives a global evaluation of the prediction quality. Second the
334 root mean squared error (RMSE) provides information about the accuracy of the
335 prediction in an absolute scale, and the relative RMSE (RRMSE) removes the impact of
336 each site's order of magnitude from the RMSE computation. Finally, the bias (BIAS) and
337 the relative bias (RBIAS) provide a measure of the magnitude of the systematic
338 overestimation or underestimation of a model.

339 **4. Case study and datasets**

340 The dataset considered in the present paper consists in 151 hydrometric stations
341 located in the southern part of the province of Quebec, Canada (Figure 3). Two versions
342 of the datasets with different variables are considered. The first is a standard one (STA)
343 with only well-known variables used in previous RFA studies (e.g. Shu et al., 2007,
344 Chebana et al., 2014, Durocher et al., 2016, Ouali et al., 2016, Wazneh et al., 2013; 2015
345 and 2016). Note that geographical coordinates of the stations are considered instead of
346 the geographical coordinates of the centroids. The second is an extended dataset (EXTD)
347 combining STA with less common variables characterizing the drainage network
348 systems. Table 2 lists all variables considered as well as whether they are in the EXTD
349 dataset and thorough definitions of the new variables can be found in (e.g. Adhikary and
350 Dash, 2018). These new variables are calculated based on drainage networks extracted
351 using the D8 approach implemented in Arc Gis (Arc Hydro) using the digital elevation
352 models; DEMs (Jenson and Domingue, 1988; O'Callaghan and Mark, 1984; Tarboton et
353 al., 1991). This method consists in calculating the flow direction and the flow

354 accumulation layers based on the direction of the steepest slope among the eight
355 neighbors of a given DEM. Using this information, the drainage networks can be defined
356 considering a constant threshold value which represents the stream head locations
357 (O'Callaghan and Mark, 1984). Descriptive statistics of the new variables used in the
358 EXTD dataset (Msilini et al., 2020) are given in Table 3. In both datasets the considered
359 hydrological response variables are at-site specific flood quantiles, chosen to match the
360 specific return periods of 10, 50 and 100 years. These quantiles are thus denoted by QS_{10} ,
361 QS_{50} and QS_{100} .

362 To ensure the convergence of the Mahalanobis distance to a χ^2 distribution in
363 CCA, note that the logarithmic transformation is used for the following variables to
364 achieve approximate normality: AREA, MBS, MATP, DDBZ and RT and a square root
365 transformation for PLAKE and RC. After transformation normal q-q plot indicate that all
366 variables are approximately normal.

367 **5. Results and Discussion**

368 **5.1 Region delineation with CCA and ROI**

369 The CCA and the ROI are applied to the DHR using two sets of variables. The first
370 set contains variables from STA, which are the area (AREA), mean basin slope (MBS),
371 percentage of the area occupied by lakes (PLAKE), mean annual total precipitation
372 (MATP), mean annual degree days below 0 °C (DDBZ) and the longitude of the centroid
373 of the basin (LONGC). The second one includes variables from the EXTD, namely
374 PLAKE, MATP, DDBZ, LONGC, texture ratio (RT) and circularity ratio (RC).

375 The obtained optimum sizes of the neighborhood are n^{opt} (STA) = 85 sites and n^{opt}
376 (EXTD) = 78 sites according to the RRMSE for the CCA method. For the ROI approach,
377 we obtain n^{opt} (STA) = 54 sites and n^{opt} (EXTD) = 44 sites according to the same
378 criterion. Thus, these neighborhood sizes are used for each target station.

379 5.2 Selection of optimal variables

380 The selection of significant explanatory variables is applied for each specific
381 quantile (QS₁₀, QS₅₀ and QS₁₀₀) and for each estimation model (GAM and MARS). Table
382 4 summarizes the final variables for each datasets (STA and EXTD). Following the
383 application of the backward technique with GAM and MARS, we note the selection of
384 the same new variables for the two models (RN, MRL and DD). The definition of these
385 variables can be found for example in Adhikary and Dash (2018). For each quantile and
386 for each model, different combinations of variables are selected. The variables that seem
387 to be the most important are AREA, PLAKE, MCL and LONGC.

388 5.3 MARS model results

389 Figure 4 shows the variable importance graph for QS₁₀₀ obtained using the EXTD
390 (we present only the results of QS₁₀₀ to avoid repetitions). The variable with the most
391 influence for the QS₁₀₀ is the percentage of the area occupied by lakes, PLAKE. Indeed,
392 lakes act as a sponge absorbing the excess water during extreme events. Thus they may
393 have a significant effect on flood peaks.

394 Figure 5 shows the GCV R^2 (GRSq) value for the QS₁₀₀ predictions versus the
395 number of terms in the final MARS model. The GCV R^2 statistic is equivalent to the
396 ordinary R^2 statistic calculated with the variance for error replaced with the GCV statistic.

397 It allows quantifying the goodness-of-fit for models that use unobserved data. The vertical
398 dashed lined at 12 indicates the optimal number of terms retained where marginal
399 increases in GCV R^2 are less than 0.001. The twelve final terms include seven variables
400 in this case. Five terms are related to interaction effects.

401 **5.4 Comparison between MARS and GAM models**

402 Table 5 shows the jackknife results for each model combination. The comparison of
403 GAM and MARS models confirms that the simple linear spline fitting generated by
404 MARS captures more information from the EXT D than the more sophisticated smoothing
405 functions used in GAM. Indeed, MARS adds the terms in an iterative way leading to a
406 simple and performant model including the effects of interactions. This model performs
407 well with the ROI which contains a smaller number of stations than CCA. Thus, based on
408 the results of our case study MARS seems applicable in small neighborhoods even with
409 complex terms (interaction effects) and able to give good predictions with fewer stations
410 than GAM.

411 The response functions fitted by GAM and MARS models for selected explanatory
412 variables are given in Figure 6. It can be seen that the smoothing functions fitted by
413 MARS approximate closely the more continuous smooth curves fitted by GAM, in a
414 simpler way. This result has been observed by Leathwick et al. (2006) in a comparative
415 study made between GAM and MARS applied in the field of ecology. The smooth curves
416 generated by GAM add degrees of freedom to the model which makes it relatively more
417 complex. This may be the reason for the better prediction results obtained by MARS than
418 GAM.

419 Figure 7 illustrates the interaction effects between some explanatory variables fitted
420 by GAM and MARS models. Note that we considered the same interactions
421 automatically identified by MARS to be able to make the comparison. The interaction
422 surface generated by both models is also close. GAM gives more continuous and
423 complex interaction effects, which lead to a large model with a large number of
424 coefficients. This makes it difficult or impossible to integrate the interaction effects with
425 GAM if we have a large number of explanatory variables in the model. For example, for
426 the QS_{100} , the integration of the same interactions identified by MARS to GAM
427 considering the same variables gives a model with 79 coefficients, versus only 12 using
428 MARS. In addition, MARS searches for and integrates interaction effects automatically
429 into the model, which allows obtaining flood quantile estimates overall better than those
430 obtained by GAM. We take as a simple example of interaction the first effect illustrated
431 in Figure 7 which represents the predicted response (specific quantile) as DD and
432 LONGC vary. It can be seen that the LONGC affects little the hydrological variable level
433 unless the DD is high where a nonlinear effect is seen.

434 **5.5 Comparison of regional models**

435 According to Table 5 (see above), the highest NASH values (0.80) and the lowest
436 RRMSE values (28.30 % for QS_{100}) are given by the ROI/MARS/EXTD, which leads to
437 the most accurate estimates compared to all other combinations. It can also be seen that,
438 with ALL, MARS has a comparable performance to GAM considering both databases.
439 However, using the neighborhoods, especially the ROI, MARS overall outperforms
440 GAM in terms of RRMSE and RBIAS criteria. This may be attributable to the flexibility
441 of MARS and its generalization ability in small size neighborhoods.

442 Figure 8 illustrates the relative error, which is the most important criterion
443 (Hosking and Wallis, 2005), as a function of the sites ordered according to their area
444 associated to the best models (ROI/MARS/EXTD and ROI/GAM/EXTD). One can
445 notice that, overall, MARS with the EXTD performs better than GAM. The figure also
446 shows that the performances at the level of extreme size basins are much worse than
447 those obtained at the level of medium size basins.

448 Figure 9 presents the differences between relative errors of MARS and GAM
449 calculated using ROI/EXTD. One can notice that, in terms of RRMSE, MARS
450 outperforms GAM in 84 sites out of 151, which represents 56% of the total number of
451 sites. Accordingly, MARS is shown to be a simple performant model that can be
452 considered as an alternative RE model.

453

454 **6. Conclusions**

455 The aim of this study is to introduce MARS in the RFA of extreme hydrological
456 variables and to compare its performance to GAM. The MARS model is able to model
457 complex relationship between physio-meteorological variables, including variables
458 dealing with drainage network characteristics, and flood quantiles at ungauged sites.

459 MARS is hereby compared to the GAM which is gaining popularity in RFA and is
460 one of the best performing models. Results show that slightly better flood quantile
461 estimates are obtained from regional models that combine MARS with the EXTD
462 including a STA with additional variables dealing with drainage network proprieties.
463 Results indicate also that better performances are obtained with the ROI which includes

464 low density of stations than CCA. This suggests that MARS is able to transfer
465 hydrological information adequately even with fewer data than GAM. Further efforts are
466 required to generalize this conclusion and to evaluate the benefits of MARS in other
467 study areas and with other hydrological variables.

468 Although MARS is an effective and simple tool for estimation that can be used in
469 RFA, there are some constraints such as the maximum number of terms and the
470 maximum allowable degree of interaction in the forward pass that have to be specified by
471 the user. These depend on the problem at hand and should be considered carefully. In
472 addition, MARS does not cope well with missing data and, like many machine learning
473 algorithms, is prone to overfitting. Note however that the backward deletion phase is
474 meant to address this drawback

475 Aside from the above-mentioned shortcomings, MARS is easy-to-use as shown in
476 this work. It is able to addresses the issues of high number of variables, nonlinearity, and
477 interactions involved in the hydrological phenomena. This yields flood quantile estimates
478 that compete with those obtained from GAM, while being simpler and more applicable to
479 smaller datasets. Flood quantiles represent important information that is used in the
480 design of hydraulic structures (e.g. dams). The construction of these structures is very
481 expensive. The availability of simple and sophisticated tools for the reliable estimation of
482 flood quantiles is crucial for hydraulics engineers.

483 In this work we considered linear neighborhood approaches (CCA and ROI), which
484 are the most used methods in RFA. Future efforts can focus on the assessment of the
485 performance of the MARS model in combination with non-linear neighborhood

486 approaches such as the non-linear canonical correlation analysis (Ouali et al., 2016) and
487 the nonlinear neighborhood based on the statistical depth function (Wazneh et al., 2016).

488 **Acknowledgments**

489 Financial support for the present study was graciously provided by the Natural Sciences
490 and Engineering Research Council of Canada (NSERC) and the Canada Research chairs
491 program (CRC). The authors are grateful to Natural Resources Canada and the USGS
492 services for the employed DEM data. The authors would like also to thank the Ministry
493 of Sustainable Development, Environment, and Fight Against Climate Change
494 (MDDELCC) services for the employed dataset (STA). The authors would like to thank
495 the Editor, Prof. Andrew Wood and three anonymous reviewers for their comments
496 which helped improve the quality of the manuscript.

497

498

499

500

501

502

503

504

505

506

507

508

509

510

511

512

513 **Appendix**

514 **Abbreviations**

ANN	Artificial neural network
AREA	Basin area
BH	Basin relief
BIAS	Mean bias
CCA	Canonical correlation analysis
DD	Drainage density
DDBZ	Mean annual degree days below 0 °C
DEM	Digital elevation model
DHR	Delineation of homogenous regions
Edf	Estimated smooth degree of freedom
EXTD	Extended dataset
FS	Stream frequency
GAM	Generalized additive model
GCV	Generalized cross validation
IF	Infiltration number
LATC	Latitude of the centroid of the basin
LONGC	Longitude of the centroid of the basin
MALP	Mean annual liquid precipitation
MALPS	Mean annual liquid precipitation (summer–fall)
MARS	Multivariate adaptive regression splines
MASP	Mean annual solid precipitation
MATP	Mean annual total precipitation
MBS	Mean basin slope
MCL	Main channel length
MCS	Main channel slope
MRB	Mean bifurcation ratio
MRL	Mean stream length ratio
NASH	Nash efficiency criterion
NL-CCA	Nonlinear canonical correlation analysis
PFOR	Percentage of the area occupied by forest
PL1	Percentage of first-order stream lengths
PLAKE	Percentage of the area occupied by lakes
PN1	Percentage of first-order streams
QS _T	Specific quantile associated to the return period T
R ²	Coefficient of determination
RB	Bifurcation ratio
RBIAS	Relative mean bias
RC	Circularity ratio
RE	Regional estimation
RFA	Regional frequency analysis
RL	Stream length ratio

RMSE	Root-mean-square error
RN	Ruggedness number
ROI	Region of influence
RRMSE	Relative root-mean-square error
RSS	Residual sum of squares
RT	Texture ratio
STA	Standard dataset
WMRB	Weighted mean bifurcation ratio

515

516 References

- 517 Adhikary, & Dash. (2018). Morphometric analysis of Katra Watershed of Eastern Ghats: A GIS
518 approach. *Int. J. Curr. Microbiol. App. Sci*, 7(3), 1651-1665.
- 519 Aziz, Rahman, Fang, & Shrestha. (2014). Application of artificial neural networks in regional
520 flood frequency analysis: a case study for Australia. *Stochastic environmental research
521 and risk assessment.*, 28(3), 541-554. doi:<https://doi.org/10.1007/s00477-013-0771-5>
- 522 Balshi, McGUIRE, Duffy, Flannigan, Walsh, & Melillo. (2009). Assessing the response of area
523 burned to changing climate in western boreal North America using a Multivariate
524 Adaptive Regression Splines (MARS) approach. *Global Change Biology*, 15(3), 578-600.
525 doi:<https://doi.org/10.1111/j.1365-2486.2008.01679.x>
- 526 Bayentin, El Adlouni, Ouarda, Gosselin, Doyon, & Chebana. (2010). Spatial variability of
527 climate effects on ischemic heart disease hospitalization rates for the period 1989-2006 in
528 Quebec, Canada. *International journal of health geographics*, 9(1), 5.
529 doi:<https://doi.org/10.1186/1476-072X-9-5>
- 530 Bishop. (1995). *Neural networks for pattern recognition*: Oxford university press.
- 531 Bond, & Kennard. (2017). Prediction of hydrologic characteristics for ungauged catchments to
532 support hydroecological modeling. *Water Resources Research*, 53(11), 8781-8794.
533 doi:<https://doi.org/10.1002/2017WR021119>
- 534 Booker, & Woods. (2014). Comparing and combining physically-based and empirically-based
535 approaches for estimating the hydrology of ungauged catchments. *Journal of Hydrology*,
536 508, 227-239.
- 537 Breiman. (2001). Random forests. *Machine learning*, 45(1), 5-32.
- 538 Brunner, Furrer, Sikorska, Viviroli, Seibert, & Favre. (2018). Synthetic design hydrographs for
539 ungauged catchments: a comparison of regionalization methods. *Stochastic
540 environmental research and risk assessment*, 32(7), 1993-2023.
- 541 Burn. (1990a). An appraisal of the "region of influence" approach to flood frequency analysis.
542 *Hydrological sciences journal.*, 35(2), 149-165.
543 doi:<https://doi.org/10.1080/02626669009492415>
- 544 Burn. (1990b). Evaluation of regional flood frequency analysis with a region of influence
545 approach. *Water Resources Research*, 26(10), 2257-2265. doi:
546 <https://doi.org/10.1029/WR026i010p02257>
- 547 Chebana, Charron, Ouarda, & Martel. (2014). Regional frequency analysis at ungauged sites with
548 the generalized additive model. *Journal of Hydrometeorology*, 15(6), 2418-2428.
549 doi:<https://doi.org/10.1175/JHM-D-14-0060.1>
- 550 Chebana, & Ouarda. (2008). Depth and homogeneity in regional flood frequency analysis. *Water
551 Resources Research*, 44(11). doi:<https://doi.org/10.1029/2007WR006771>
- 552 Cutler, Edwards Jr, Beard, Cutler, Hess, Gibson, & Lawler. (2007). Random forests for
553 classification in ecology. *Ecology*, 88(11), 2783-2792.

554 Deo, Kisi, & Singh. (2017). Drought forecasting in eastern Australia using multivariate adaptive
555 regression spline, least square support vector machine and M5Tree model. *Atmospheric*
556 *Research*, 184, 149-175. doi:<https://doi.org/10.1016/j.atmosres.2016.10.004>
557 Diez-Sierra, & del Jesus. (2019). Subdaily rainfall estimation through daily rainfall downscaling
558 using random forests in Spain. *Water*, 11(1), 125.
559 Emamgolizadeh, Bateni, Shahsavani, Ashrafi, & Ghorbani. (2015). Estimation of soil cation
560 exchange capacity using genetic expression programming (GEP) and multivariate
561 adaptive regression splines (MARS). *Journal of Hydrology*, 529, 1590-1600.
562 doi:<https://doi.org/10.1016/j.jhydrol.2015.08.025>
563 Friedman. (1991). Multivariate adaptive regression splines. *The annals of statistics*, 1-67.
564 Gal, & Ghahramani. (2016). *A theoretically grounded application of dropout in recurrent neural*
565 *networks*. Paper presented at the Advances in neural information processing systems.
566 Geurts, Irtthum, & Wehenkel. (2009). Supervised learning with decision tree-based methods in
567 computational and systems biology. *Molecular Biosystems*, 5(12), 1593-1605.
568 GREHYS. (1996). Presentation and review of some methods for regional flood frequency
569 analysis. *Journal of hydrology(Amsterdam)*, 186(1-4), 63-84.
570 Hastie, & Tibshirani. (1987). Generalized Additive Models: Some Applications. *Journal of the*
571 *American statistical Association*, 82(398), 371-386.
572 doi:10.1080/01621459.1987.10478440
573 Hosking, & Wallis. (2005). *Regional frequency analysis: an approach based on L-moments*:
574 Cambridge University Press.
575 Hotelling. (1935). Canonical correlation analysis (cca). *Journal of Educational Psychology*, 10.
576 Ibbitt, & Woods. (2004). Re-scaling the topographic index to improve the representation of
577 physical processes in catchment models. *Journal of Hydrology*, 293(1-4), 205-218.
578 doi:<https://doi.org/10.1016/j.jhydrol.2004.01.016>
579 Jenson, & Domingue. (1988). Extracting topographic structure from digital elevation data for
580 geographic information system analysis. *Photogrammetric engineering and remote*
581 *sensing*, 54(11), 1593-1600.
582 Jung, Marpu, & Ouarda. (2017). Impact of river network type on the time of concentration.
583 *Arabian Journal of Geosciences*, 10(24), 546. doi:[https://doi.org/10.1007/s12517-017-](https://doi.org/10.1007/s12517-017-3323-3)
584 [3323-3](https://doi.org/10.1007/s12517-017-3323-3)
585 Khalil, Ouarda, & St-Hilaire. (2011). Estimation of water quality characteristics at ungauged sites
586 using artificial neural networks and canonical correlation analysis. *Journal of Hydrology*,
587 405(3-4), 277-287.
588 Kisi. (2015). Pan evaporation modeling using least square support vector machine, multivariate
589 adaptive regression splines and M5 model tree. *Journal of Hydrology*, 528, 312-320.
590 doi:<https://doi.org/10.1016/j.jhydrol.2015.06.052>
591 Kisi, & Parmar. (2016). Application of least square support vector machine and multivariate
592 adaptive regression spline models in long term prediction of river water pollution.
593 *Journal of Hydrology*, 534, 104-112. doi:<https://doi.org/10.1016/j.jhydrol.2015.12.014>
594 Lawrence, & Giles. (2000). *Overfitting and neural networks: conjugate gradient and*
595 *backpropagation*. Paper presented at the Proceedings of the IEEE-INNS-ENNS
596 International Joint Conference on Neural Networks. IJCNN 2000. Neural Computing:
597 New Challenges and Perspectives for the New Millennium.
598 Leathwick, Elith, & Hastie. (2006). Comparative performance of generalized additive models and
599 multivariate adaptive regression splines for statistical modelling of species distributions.
600 *Ecological Modelling*, 199(2), 188-196.
601 doi:<https://doi.org/10.1016/j.ecolmodel.2006.05.022>
602 Leathwick, Rowe, Richardson, Elith, & Hastie. (2005). Using multivariate adaptive regression
603 splines to predict the distributions of New Zealand's freshwater diadromous fish.

604 *Freshwater Biology*, 50(12), 2034-2052. doi:[https://doi.org/10.1111/j.1365-](https://doi.org/10.1111/j.1365-2427.2005.01448.x)
605 [2427.2005.01448.x](https://doi.org/10.1111/j.1365-2427.2005.01448.x)

606 Leclerc, & Ouarda. (2007). Non-stationary regional flood frequency analysis at ungauged sites.
607 *Journal of Hydrology*, 343(3-4), 254-265.
608 doi:<https://doi.org/10.1016/j.jhydrol.2007.06.021>

609 Lee, & Chen. (2005). A two-stage hybrid credit scoring model using artificial neural networks
610 and multivariate adaptive regression splines. *Expert Systems with Applications*, 28(4),
611 743-752. doi:<https://doi.org/10.1016/j.eswa.2004.12.031>

612 Lee, Chiu, Chou, & Lu. (2006). Mining the customer credit using classification and regression
613 tree and multivariate adaptive regression splines. *Computational Statistics & Data*
614 *Analysis*, 50(4), 1113-1130. doi:<https://doi.org/10.1016/j.csda.2004.11.006>

615 Leitte, Petrescu, Franck, Richter, Suci, Ionovici, et al. (2009). Respiratory health, effects of
616 ambient air pollution and its modification by air humidity in Drobeta-Turnu Severin,
617 Romania. *Science of The Total Environment*, 407(13), 4004-4011.
618 doi:<https://doi.org/10.1016/j.scitotenv.2009.02.042>

619 Li, He, Su, & Shu. (2016). Forecasting the daily power output of a grid-connected photovoltaic
620 system based on multivariate adaptive regression splines. *Applied Energy*, 180, 392-401.
621 doi:<https://doi.org/10.1016/j.apenergy.2016.07.052>

622 Masselink, Temme, Giménez Díaz, Casali Sarasibar, & Keesstra. (2017). Assessing hillslope-
623 channel connectivity in an agricultural catchment using rare-earth oxide tracers and
624 random forests models. *Cuadernos de Investigación Geográfica 2017, n° 43 (1)*, pp. 19-
625 39.

626 Milborrow. (2018). Derived from MDA: mars by Trevor Hastie and Rob Tibshirani. Uses Alan
627 Miller's Fortran utilities with Thomas Lumley's leaps wrapper. Earth: Multivariate
628 Adaptive Regression Splines . R package version 4.6.3.

629 Msilini, Ouarda, & Masselot. (2020). Evaluation of additional physiographical variables
630 characterising drainage network systems in regional frequency analysis, a Quebec
631 watersheds case-study. *Manuscript submitted for publication*.

632 Muñoz, Orellana-Alvear, Willems, & Céleri. (2018). Flash-flood forecasting in an Andean
633 mountain catchment—Development of a step-wise methodology based on the random
634 forest algorithm. *Water*, 10(11), 1519.

635 Niehoff, Fritsch, & Bronstert. (2002). Land-use impacts on storm-runoff generation: scenarios of
636 land-use change and simulation of hydrological response in a meso-scale catchment in
637 SW-Germany. *Journal of Hydrology*, 267(1-2), 80-93. doi:[https://doi.org/10.1016/S0022-](https://doi.org/10.1016/S0022-1694(02)00142-7)
638 [1694\(02\)00142-7](https://doi.org/10.1016/S0022-1694(02)00142-7)

639 O'Callaghan, & Mark. (1984). The extraction of drainage networks from digital elevation data.
640 *Computer vision, graphics, and image processing*, 28(3), 323-344.
641 doi:[https://doi.org/10.1016/S0734-189X\(84\)80011-0](https://doi.org/10.1016/S0734-189X(84)80011-0)

642 Ouali, Chebana, & Ouarda. (2016). Non-linear canonical correlation analysis in regional
643 frequency analysis. *Stochastic environmental research and risk assessment*, 30(2), 449-
644 462. doi:<https://doi.org/10.1007/s00477-015-1092-7>

645 Ouali, Chebana, & Ouarda. (2017). Fully nonlinear statistical and machine-learning approaches
646 for hydrological frequency estimation at ungauged sites. *Journal of Advances in*
647 *Modeling Earth Systems*, 9(2), 1292-1306. doi:<https://doi.org/10.1002/2016MS000830>

648 Ouarda. (2016). Regional flood frequency modeling. *chapter 77, in: V.P. Singh, (Ed). Chow's*
649 *Handbook of Applied Hydrology, 3rd Edition, Mc-Graw Hill, New York*, pp. 77.71-77.78,
650 ISBN 978-970-907-183509-183501.

651 Ouarda, Charron, Hundecha, St-Hilaire, & Chebana. (2018). Introduction of the GAM model for
652 regional low-flow frequency analysis at ungauged basins and comparison with commonly
653 used approaches. *Environmental Modelling & Software*, 109, 256-271.
654 doi:<https://doi.org/10.1016/j.envsoft.2018.08.031>

655 Ouarda, Charron, Marpu, & Chebana. (2016). The generalized additive model for the assessment
656 of the direct, diffuse, and global solar irradiances using SEVIRI images, with application
657 to the UAE. *IEEE Journal of Selected Topics in Applied Earth Observations and Remote*
658 *Sensing*, 9(4), 1553-1566. doi:<https://doi.org/10.1109/jstars.2016.2522764>

659 Ouarda, Girard, Cavadias, & Bobée. (2001). Regional flood frequency estimation with canonical
660 correlation analysis. *Journal of Hydrology*, 254(1), 157-173.
661 doi:[https://doi.org/10.1016/S0022-1694\(01\)00488-7](https://doi.org/10.1016/S0022-1694(01)00488-7)

662 Ouarda, Lang, Bobée, Bernier, & Bois. (1999). Synthèse de modèles régionaux d'estimation de
663 crue utilisée en France et au Québec. *Revue des sciences de l'eau/Journal of Water*
664 *Science*, 12(1), 155-182. doi:<https://doi.org/10.7202/705347ar>

665 Ouarda, & Shu. (2009). Regional low-flow frequency analysis using single and ensemble
666 artificial neural networks. *Water Resources Research*, 45(11).
667 doi:<https://doi.org/10.1029/2008wr007196>

668 Pourghasemi, & Kerle. (2016). Random forests and evidential belief function-based landslide
669 susceptibility assessment in Western Mazandaran Province, Iran. *Environmental Earth*
670 *Sciences*, 75(3), 185.

671 Prasad, Iverson, & Liaw. (2006). Newer classification and regression tree techniques: bagging
672 and random forests for ecological prediction. *Ecosystems*, 9(2), 181-199.

673 Quenouille. (1949). Problems in plane sampling. *The Annals of Mathematical Statistics*, 20(3),
674 355-375. doi:10.1214/aoms/1177729989

675 Rahman, Charron, Ouarda, & Chebana. (2018). Development of regional flood frequency
676 analysis techniques using generalized additive models for Australia. *Stochastic*
677 *environmental research and risk assessment*, 32(1), 123-139.
678 doi:<https://doi.org/10.1007/s00477-017-1384-1>

679 Ramsay, Burnett, & Krewski. (2003). The effect of concavity in generalized additive models
680 linking mortality to ambient particulate matter. *Epidemiology*, 14(1), 18-23.

681 Rounaghi, Abbaszadeh, & Arashi. (2015). Stock price forecasting for companies listed on Tehran
682 stock exchange using multivariate adaptive regression splines model and semi-parametric
683 splines technique. *Physica A: Statistical Mechanics and its Applications*, 438, 625-633.
684 doi:<https://doi.org/10.1016/j.physa.2015.07.021>

685 Roy, Roy, & Balas. (2018). Estimating heating load in buildings using multivariate adaptive
686 regression splines, extreme learning machine, a hybrid model of MARS and ELM.
687 *Renewable and Sustainable Energy Reviews*, 82, 4256-4268.
688 doi:<https://doi.org/10.1016/j.rser.2017.05.249>

689 Saadi, Oudin, & Ribstein. (2019). Random Forest Ability in Regionalizing Hourly Hydrological
690 Model Parameters. *Water*, 11(8), 1540. doi:<https://doi.org/10.3390/w11081540>

691 Shu, & Burn. (2004). Artificial neural network ensembles and their application in pooled flood
692 frequency analysis. *Water Resources Research*, 40(9).
693 doi:<https://doi.org/10.1029/2003WR002816>

694 Sivakumar. (2007). Nonlinear determinism in river flow: prediction as a possible indicator. *Earth*
695 *Surface Processes and Landforms: The Journal of the British Geomorphological*
696 *Research Group*, 32(7), 969-979. doi: <https://doi.org/10.1002/esp.1462>

697 Tarboton, Bras, & Rodriguez-Iturbe. (1991). On the extraction of channel networks from digital
698 elevation data. *Hydrological Processes*, 5(1), 81-100. doi:
699 <https://doi.org/10.1002/hyp.3360050107>

700 Tasker, Hodge, & Barks. (1996). REGION OF INFLUENCE REGRESSION FOR
701 ESTIMATING THE 50-YEAR FLOOD AT UNGAGED SITES. *JAWRA Journal of the*
702 *American Water Resources Association*, 32(1), 163-170.
703 doi:<https://doi.org/10.1111/j.1752-1688.1996.tb03444.x>

704 Wahba. (1990). *Spline models for observational data* (Vol. 59): Siam.

705 Wang, Chen, Shi, & Van Gelder. (2008). Detecting changes in extreme precipitation and extreme
706 streamflow in the Dongjiang River Basin in southern China. *Hydrology and Earth System*
707 *Sciences Discussions*, 12(1), 207-221.

708 Wang, Lai, Chen, Yang, Zhao, & Bai. (2015). Flood hazard risk assessment model based on
709 random forest. *Journal of Hydrology*, 527, 1130-1141.

710 Wazneh, Chebana, & Ouarda. (2016). Identification of hydrological neighborhoods for regional
711 flood frequency analysis using statistical depth function. *Advances in water resources*,
712 94, 251-263. doi:<https://doi.org/10.1016/j.advwatres.2016.05.013>

713 Wen, Rogers, Saintilan, & Ling. (2011). The influences of climate and hydrology on population
714 dynamics of waterbirds in the lower Murrumbidgee River floodplains in Southeast
715 Australia: implications for environmental water management. *Ecological Modelling*,
716 222(1), 154-163. doi:<https://doi.org/10.1016/j.ecolmodel.2010.09.016>

717 Wood. (2003). Thin plate regression splines. *Journal of the Royal Statistical Society: Series B*
718 *(Statistical Methodology)*, 65(1), 95-114. doi:<https://doi.org/10.1111/1467-9868.00374>

719 Wood. (2004). Stable and Efficient Multiple Smoothing Parameter Estimation for Generalized
720 Additive Models. *Journal of the American statistical Association*, 99(467), 673-686.
721 doi:10.1198/016214504000000980

722 Wood. (2006). *Generalized additive models: an introduction with R*: CRC press.

723 Wood. (2017). *Generalized additive models: an introduction with R*: CRC press.

724 Xu, Li, Ji, Lu, & Dong. (2010). A comprehensive approach to characterization of the nonlinearity
725 of runoff in the headwaters of the Tarim River, western China. *Hydrological Processes:*
726 *An International Journal*, 24(2), 136-146. doi:<https://doi.org/10.1002/hyp.7484>

727 Zhang, & Goh. (2016). Evaluating seismic liquefaction potential using multivariate adaptive
728 regression splines and logistic regression. *Geomech Eng*, 10(3), 269-280.
729 doi:<http://dx.doi.org/10.12989/gae.2016.10.3.269>

730 Zhang, Goh, Zhang, Chen, & Xiao. (2015). Assessment of soil liquefaction based on capacity
731 energy concept and multivariate adaptive regression splines. *Engineering Geology*, 188,
732 29-37. doi:<https://doi.org/10.1016/j.enggeo.2015.01.009>

733

734

735

736

737

738

739

740

741

742

743

744

745

746

747

748

Table 1 Adopted regional models.

Step	DHR	RE
Regional model	STA /EXTD	
ALL/GAM	ALL (all stations)	GAM
ALL/MARS	ALL (all stations)	MARS
CCA/GAM	CCA	GAM
CCA/MARS	CCA	MARS
ROI/GAM	ROI	GAM
ROI/MARS	ROI	MARS

749

750

Table 2 Variables used in the STA and the EXTD.

QS_T	Specific quantile associated to the return period T ; (T = 10, 50 and 100 years.)	*	+	
AREA	Basin area	*	+	Log
MCL	Main channel length	*	+	
MCS	Main channel slope	*	+	
MBS	Mean basin slope	*	+	Log
PFOR	Percentage of the area occupied by forest	*	+	
PLAKE	Percentage of the area occupied by lakes	*	+	√.
MATP	Mean annual total precipitation	*	+	Log
MALP	Mean annual liquid precipitation	*	+	
MASP	Mean annual solid precipitation	*	+	
MALPS	Mean annual liquid precipitation (summer–fall)	*	+	
DDBZ	Mean annual degree days below 0 °C	*	+	Log
LATC	Latitude of the centroid of the basin	*	+	
LONGC	Longitude of the centroid of the basin	*	+	---
RT	Texture ratio		+	Log
RC	Circularity ratio		+	√.
MRL	Mean stream length ratio		+	
MRB	Mean bifurcation ratio		+	
WMRB	Weighted mean bifurcation ratio		+	
ρ_{WMRB}	RHO WMRB coefficient		+	
DD	Drainage density		+	
FS	Stream frequency		+	
IF	Infiltration number		+	
RN	Ruggedness number		+	
PN1	Percentage of first-order streams		+	

751 (*) Variables considered in the standard dataset (STA).

752 (+) Variables considered in the extended dataset (EXTD).

753 The variables considered in the neighborhoods and their transformations are presented in
 754 bold character.

755 **Table 3** Descriptive statistics of new physiographical variables.

Variable	Min	Mean	Max	STD.dev
DD (Km ⁻¹)	2.41	2.96	4.73	0.34
FS (Km ⁻²)	7.34	9.74	11.86	0.97
IF (Km ⁻³)	17.69	29.26	67.09	6.56
RT (Km ⁻¹)	8.09	32.11	131.84	21.41
MRB	1.67	2.40	17.27	2.08
WMRB	1.95	2.08	4.14	0.24
MRL	0.85	0.97	1.11	0.05
ρWMRB	0.23	0.47	0.55	0.04
RN	0.20	1.89	7.48	1.03
RC	0.06	0.18	0.46	0.08
PN1 (%)	50.12	50.41	52.50	0.30
PL1 (%)	44.09	52.89	66.36	4.10

756

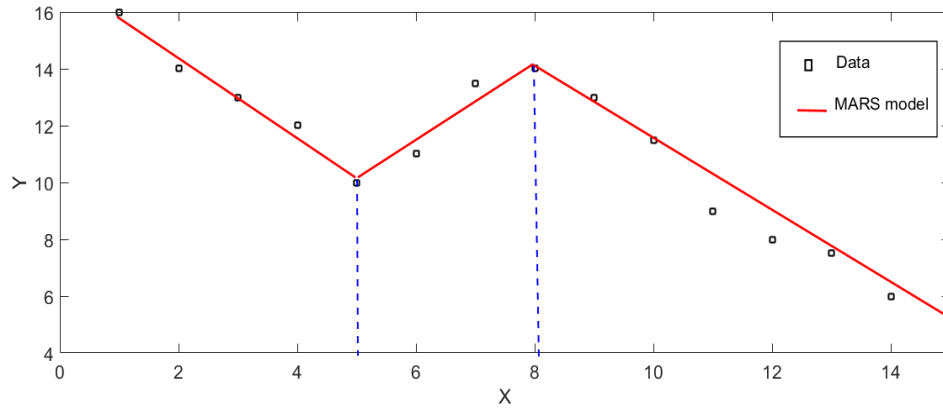
757 **Table 4** Explanatory variables selected for the various regression models.

Regional models	Quantile	Selected predictor variables
ALL/GAM/STA, CCA/GAM/STA, ROI/GAM/STA	QS ₁₀	AREA, MBS, PLAKE, MALP, MASP, DDBZ, LONGC
	QS ₅₀	AREA, MCL, MBS, PLAKE, MALP, DDBZ, LONGC
	QS ₁₀₀	AREA, MCL, MBS, PLAKE, MALP, DDBZ, LONGC
ALL/GAM/EXTD, CCA/GAM/EXTD, ROI/GAM/EXTD	QS ₁₀	MCL, PLAKE, MATP, DDBZ, DD, RN, LATC
	QS ₅₀	MCL, PLAKE, MALP, DDBZ, DD, MRL, LONGC
	QS ₁₀₀	MCL, PLAKE, MALP, DDBZ, DD, MRL, LONGC
ALL/MARS/STA, CCA/MARS/STA, ROI/MARS/STA	QS ₁₀	PLAKE, LONGC, MCL, LATC, MALP, AREA, MBS
	QS ₅₀	PLAKE, LONGC, MCL, LATC, PFOR, MASP
	QS ₁₀₀	PLAKE, LONGC, MCL, LATC, PFOR, MASP
ALL/MARS/EXTD, CCA/MARS/EXTD, ROI/MARS/EXTD	QS ₁₀	PLAKE, LONGC, MCL, DD, MRL, MALP
	QS ₅₀	PLAKE, LONGC, MCL, DD, MRL, MASP
	QS ₁₀₀	PLAKE, LONGC, MCL, LATC, DD, RN, MASP

Table 5 Jackknife Validation Results (STD and EXTD).

		STA						EXTD					
		ALL		CCA		ROI		ALL		CCA		ROI	
Quantile		GAM	MARS	GAM	MARS	GAM	MARS	GAM	MARS	GAM	MARS	GAM	MARS
NASH	QS ₁₀	0.774	0.788	0.797	0.771	0.829	0.866	0.802	0.820	0.837	0.797	0.865	0.859
	QS ₅₀	0.745	0.648	0.762	0.749	0.796	0.785	0.754	0.742	0.775	0.748	0.816	0.802
	QS ₁₀₀	0.715	0.643	0.723	0.679	0.762	0.752	0.725	0.625	0.742	0.682	0.791	0.803
RMSE [(m ³ /s)km ⁻²]	QS ₁₀	0.060	0.058	0.057	0.060	0.053	0.047	0.056	0.054	0.051	0.057	0.047	0.047
	QS ₅₀	0.089	0.104	0.086	0.088	0.080	0.081	0.087	0.089	0.080	0.088	0.076	0.076
	QS ₁₀₀	0.107	0.119	0.105	0.113	0.097	0.099	0.105	0.122	0.101	0.112	0.091	0.089
RRMSE (%)	QS ₁₀	40.937	40.781	37.163	35.316	34.690	25.950	34.970	32.065	30.619	30.435	27.974	24.423
	QS ₅₀	49.420	51.552	43.333	43.086	39.365	30.439	36.659	35.214	35.086	35.282	27.818	29.210
	QS ₁₀₀	51.832	47.953	45.678	42.298	41.661	37.775	38.630	41.215	37.416	38.818	29.235	28.298
BIAS [(m ³ /s)km ⁻²]	QS ₁₀	0.005	0.004	0.006	0.004	0.003	0.007	0.005	0.005	0.007	0.008	0.004	0.008
	QS ₅₀	0.008	0.008	0.015	0.014	0.006	0.009	0.008	0.006	0.015	0.015	0.009	0.009
	QS ₁₀₀	0.011	0.008	0.020	0.014	0.009	0.011	0.011	0.007	0.020	0.016	0.012	0.001
RBIAIS (%)	QS ₁₀	-5.461	-4.650	-5.555	-5.095	-4.177	-1.682	-4.179	-4.003	-3.871	-2.818	-2.836	-0.250
	QS ₅₀	-7.047	-8.563	-5.632	-5.778	-5.487	-3.154	-4.954	-4.862	-3.513	-3.514	-2.892	-2.176
	QS ₁₀₀	-7.663	-8.451	-5.780	-6.291	-5.816	-5.275	-5.472	-5.767	-3.714	-4.465	-3.172	-3.583

759 Best results are in bold character.



761

762

Figure 1 Knots and linear splines for a simple example of MARS.

763

764

765

766

767

768

769

770

771

772

773

774

775

776

777

778

779

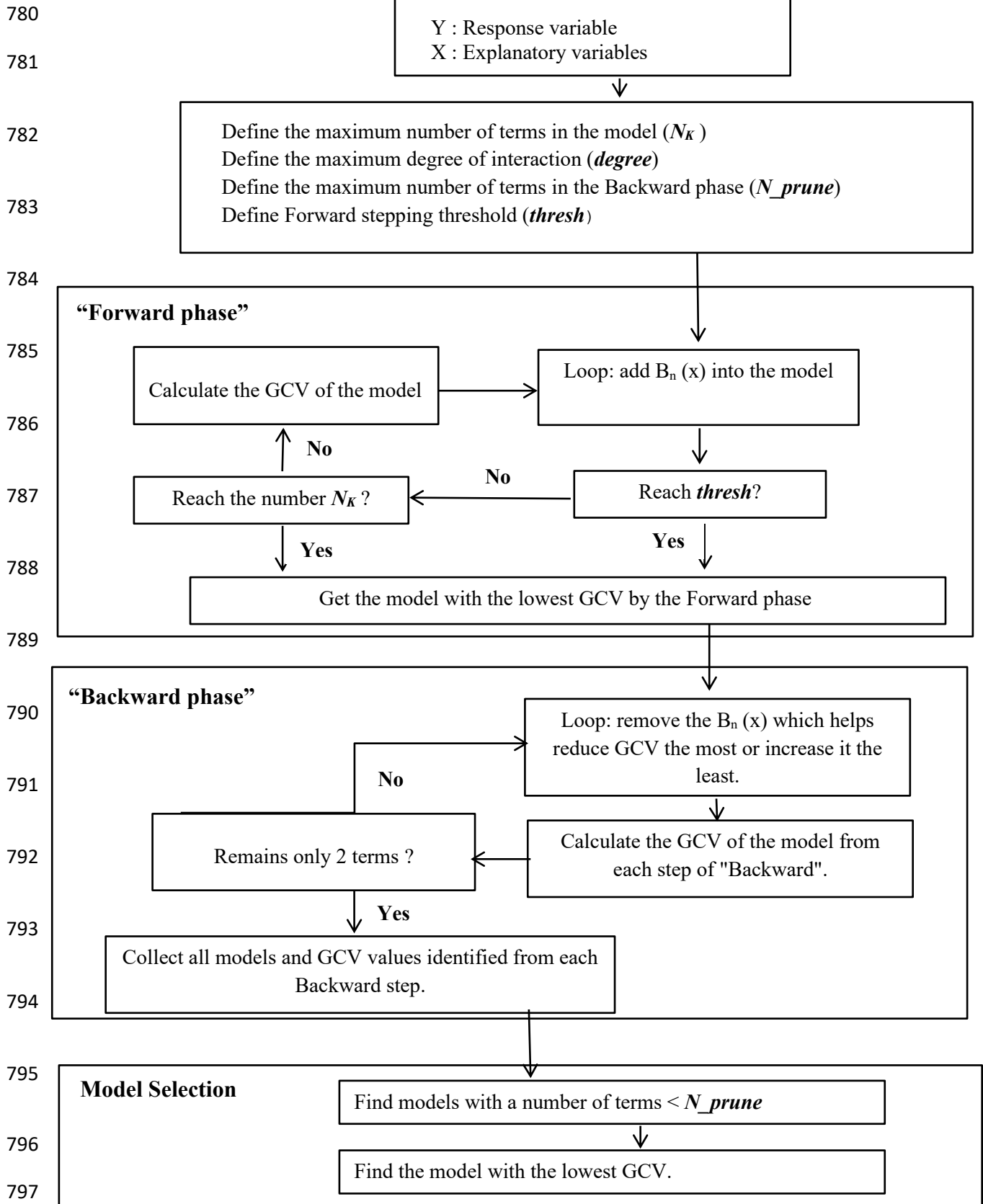
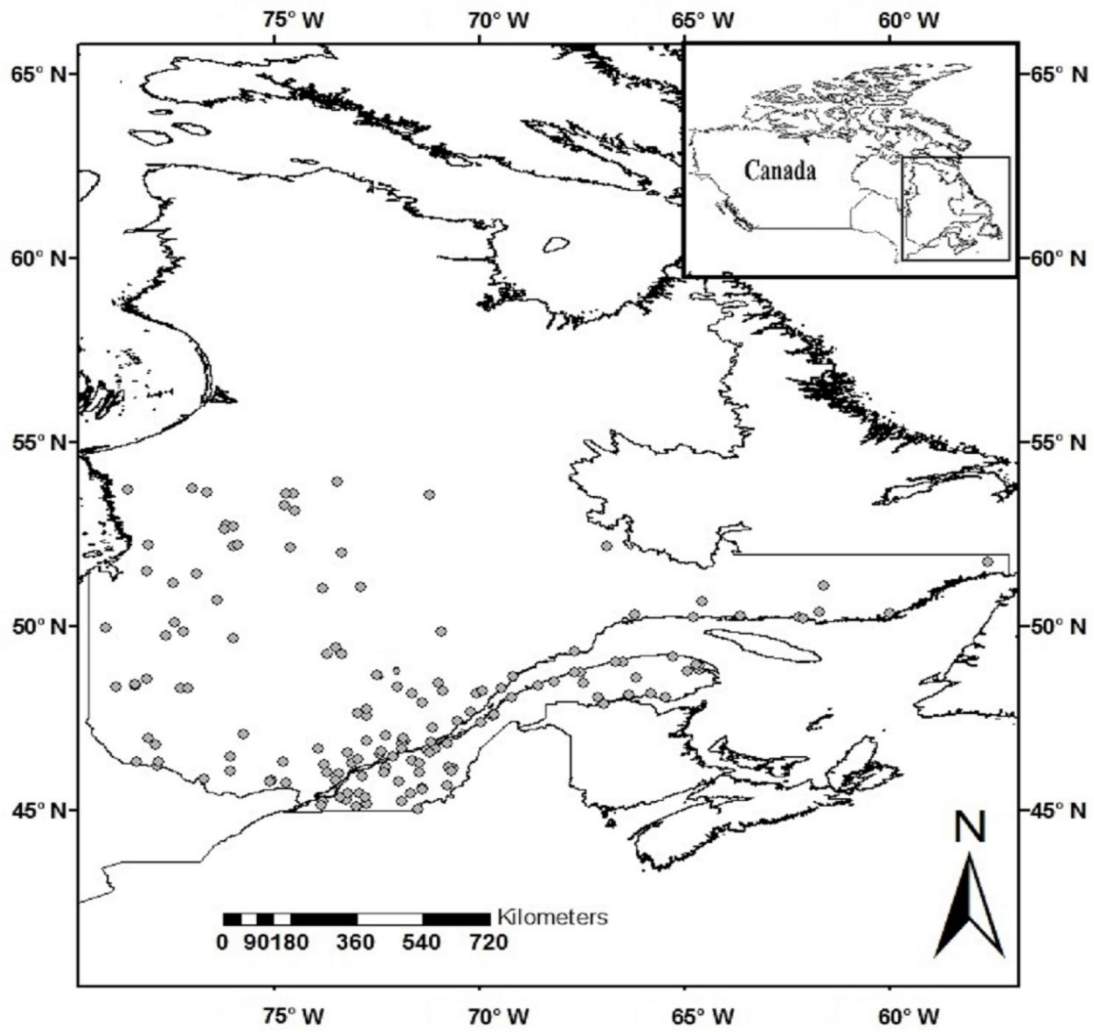


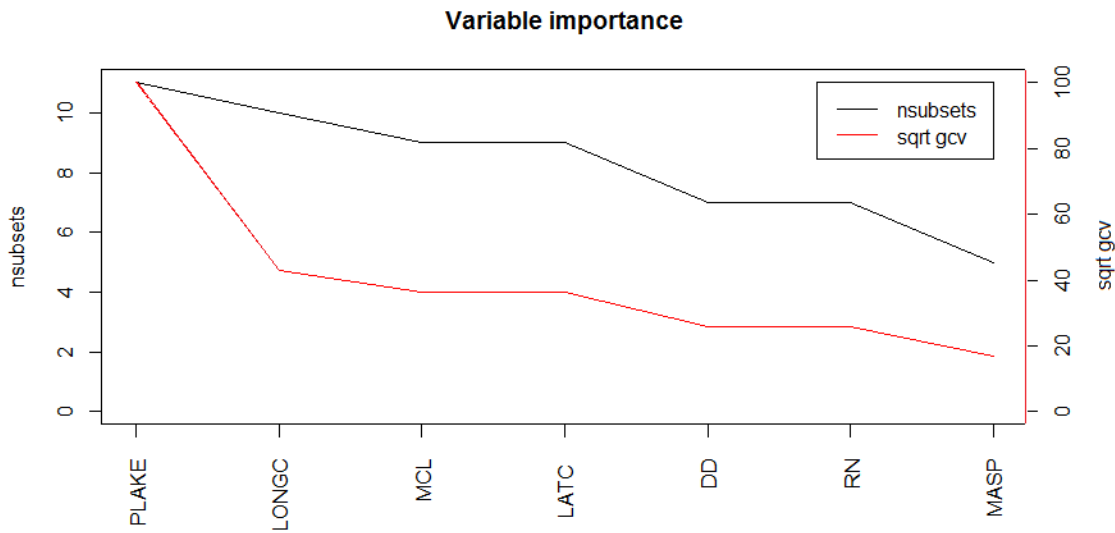
Figure 2 Graph of MARS modelling process.



798

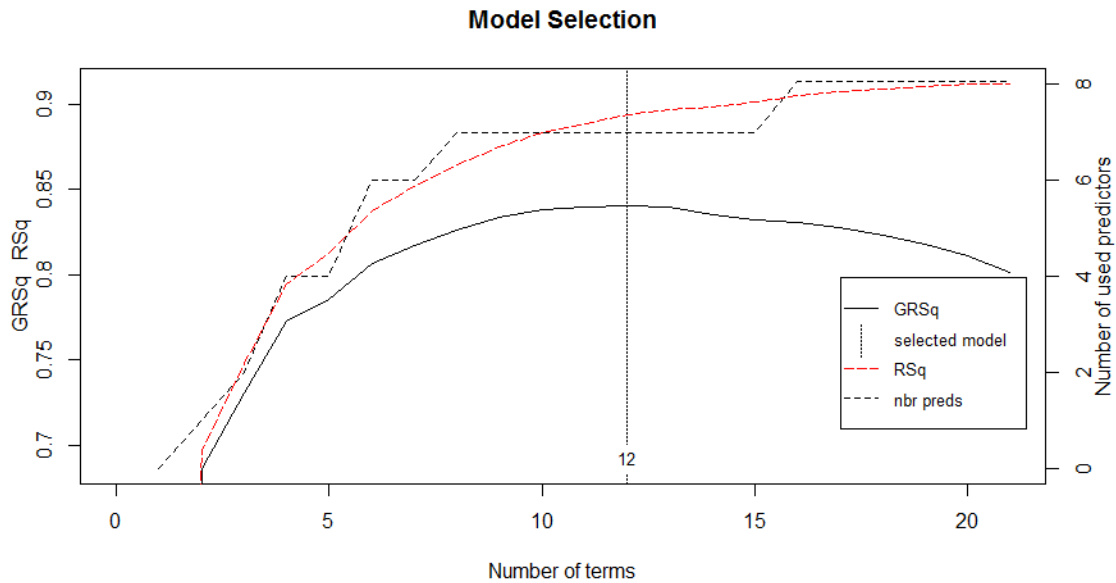
799 **Figure 3** Geographical location of the studied sites in the southern part of the province of
 800 Quebec, Canada.

801



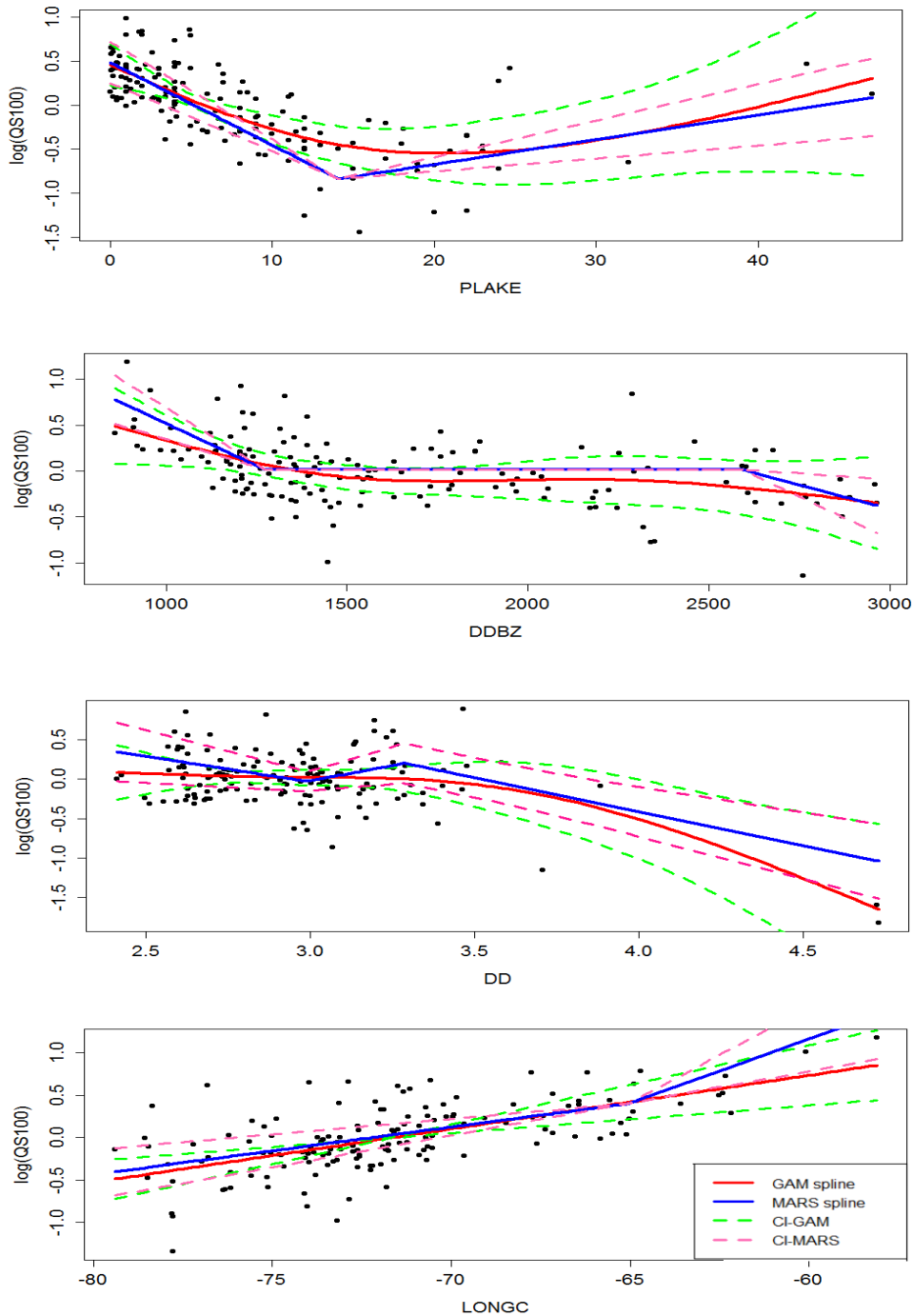
802

803 **Figure 4** Variable Importance while predicting QS_{100} . The Redline represents the variation of the
 804 sqrt GCV values caused by the removal of a given variable from the MARS model during the
 805 backward phase. The black line represents the variation of the number of sub-models including a
 806 given variable.



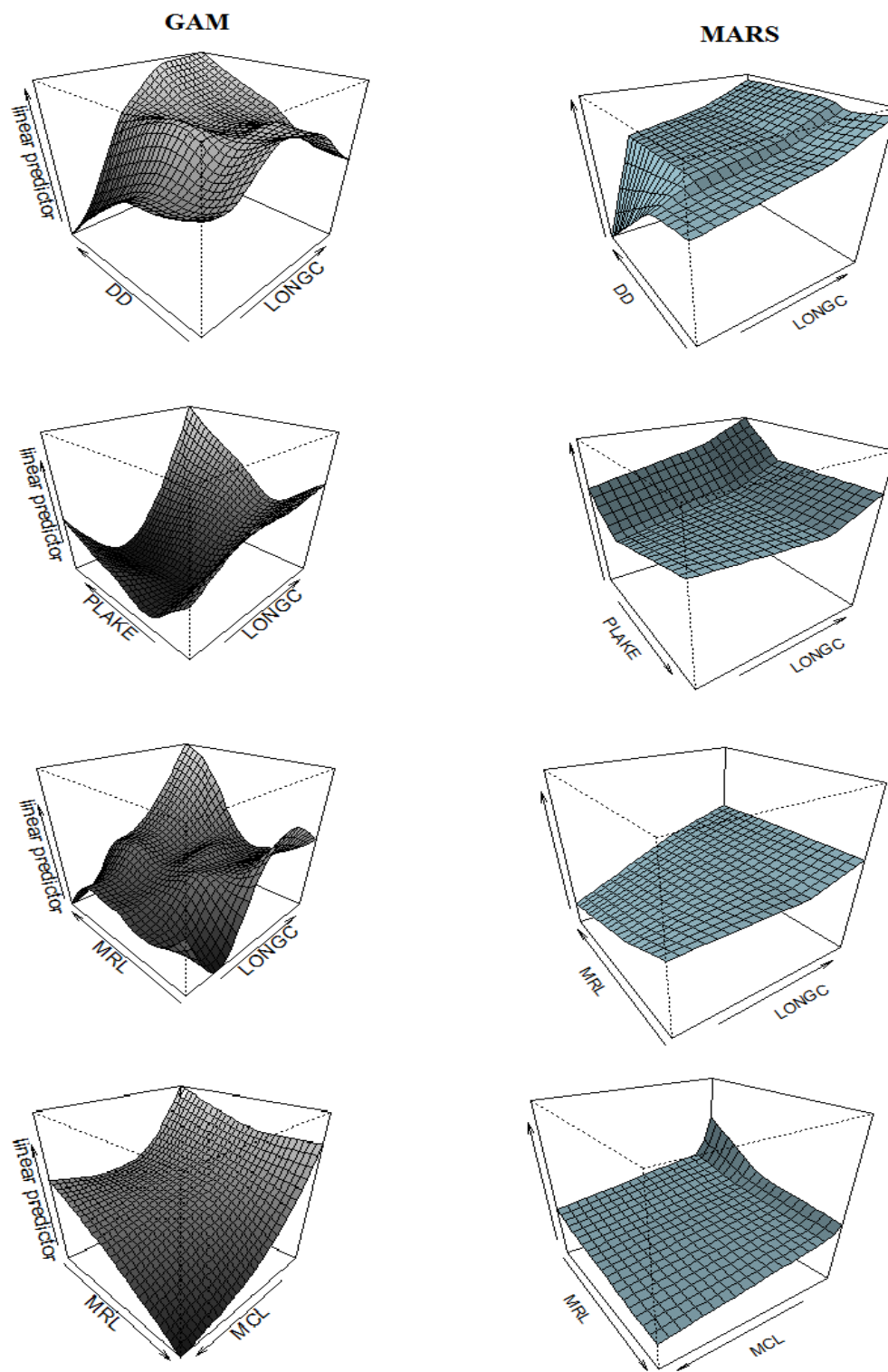
807

808 **Figure 5** MARS model selection for QS_{100} . The gray line and the red dashed line
 809 represent, respectively, the variation of the $\text{GCV } R^2$ (GRSq) and the R^2 (RSq) values in
 810 the backward phase. For this model, 12 terms were retained which are based on 7
 811 predictors (nbr preds).



812

813 **Figure 6** Examples of smoothing functions produced by the GAM and MARS models for some
 814 explanatory variables. Dashed lines represent the 95% confidence intervals (CI). A Bayesian
 815 approach to variance estimation is used to calculate the CI for GAM. For MARS, the approach
 816 considered to identify the CI for MARS is the one that we can use for a linear regression model as
 817 it is simply a linear regression of linear basis functions. All the terms are estimated with a sum to
 818 zero constraint, leading to lower uncertainty associated with the mean in the plots.

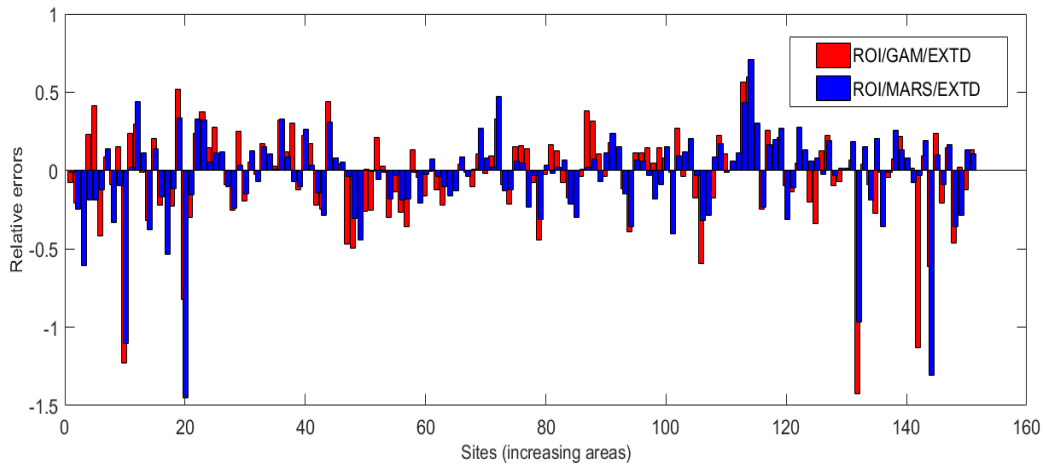


819

820

821

Figure 7 Examples of the multivariate effects of some explanatory variables produced by the GAM and MARS models on the response variable (interactions).



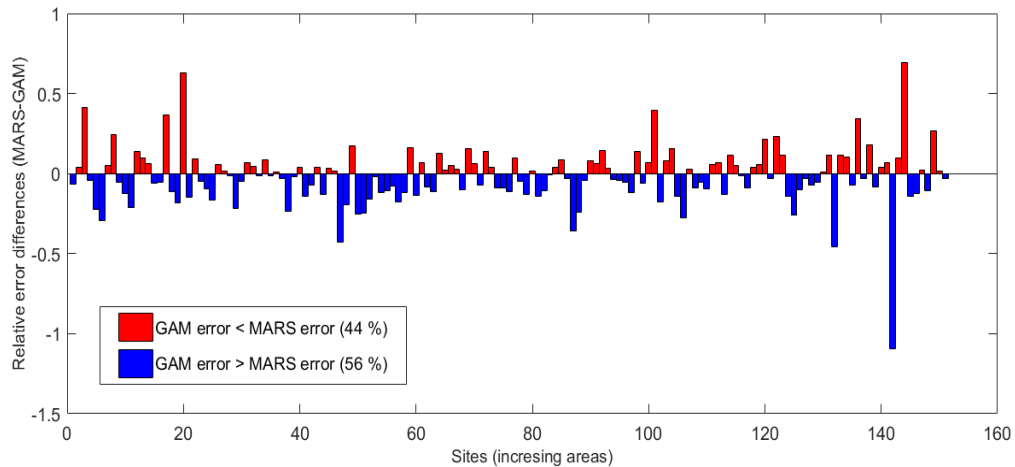
822

823

824

Figure 8 Relative errors associated to the at site quantile QS_{100} calculated using ROI/GAM/EXTD and ROI/MARS/EXTD.

825



826

827

828

829

830

831

832

833

834

Figure 9 Relative errors differences associated to the at site quantile QS_{100} calculated between MARS and GAM. The considered combinations are ROI/GAM/EXTD and ROI/MARS/EXTD.